Toward a Generalized Algorithm for the Modeling of the Dispersive Properties of Integrated Circuit Structures on Anisotropic Substrates

AKIFUMI NAKATANI, STUDENT MEMBER, IEEE, AND NICÓLAOS G. ALEXÓPOULOS, SENIOR MEMBER, IEEE

Abstract—**A variety of substrate materials used in practice exhibit anisotropic behavior which is either inherent to the material or may be acquired during the manufacturing process. The development of highly accurate models for the propagation properties of integrated circuit structures necessitates careful accounting of substrate anisotropy. In this paper, an algorithm is developed which models structures such as microstrip, inverted microstrip, slotlines, and coplanar waveguides on anisotropic substrates. The model includes cases where the circuit has a cover or is enclosed in a rectangular shield.**

I. Introduction

ANISOTROPY IS either an inherent property of a substrate material or may be acquired during the manufacturing process. Uniaxial crystalline substrates (such as, e.g., sapphire and quartz) belong to the former while fiber or ceramic impregnated plastics (such as, e.g., Epsilam-10) belong to the latter category. It has been clarified that when anisotropy is ignored in the development of design methods for single and coupled microstrip on Epsilam-10, an error is introduced which becomes significant for small linewidths and small line separation [1]. It follows that the development of highly accurate models for integrated circuit structures should account for substrate anisotropy. In addition, in certain applications of coupled line structures, anisotropy may prove beneficial in equalizing even–odd-mode phase velocities and reducing geometry tolerance sensitivity [2]. The dispersive behavior of microstrip [3]–[5], coupled slots [6], and coplanar waveguides [7] has been investigated to some extent including the case of microstrip discontinuities. This paper addresses the problem in a more generalized fashion in that a technique is developed which may encompass all useful structures with or without cover or with a rectangular shield. Furthermore, the algorithm discussed in this paper includes the possibility of multiple anisotropic layers, each of which is characterized by a diagonalized tensor permittivity $\bar{\bar{\epsilon}}$. The method consists of developing the LSE- and LSM-mode field solution to derive the Green's function for the structure under consideration. Subsequently, the Galerkin method is used to obtain the longitudinal and transverse current density or aperture electric-field components. In this manner, the dispersive behavior of several structures is obtained to show the versatility of the method. The error introduced when anisotropy is neglected is also discussed.

Manuscript received March 18, 1985; revised August 9, 1985. This work was supported in part by the National Science Foundation under Contract ECS 82-15408.

The authors are with the Electrical Engineering Department, University of California, Los Angeles, Los Angeles, CA 90024.

II. The Fourier Series Spectrum Method

The typical structures under consideration are shown in Fig. 1, where coupled microstrip and coplanar waveguide geometries are depicted with multiple anisotropic layers. The relative permittivity of the ith layer is given by

$$\bar{\bar{\epsilon}}^{(i)} = \begin{pmatrix} \epsilon_t^{(i)} & 0 & 0 \\ 0 & \epsilon_{yy}^{(i)} & 0 \\ 0 & 0 & \epsilon_t^{(i)} \end{pmatrix} \tag{1}$$

where $\epsilon_t^{(i)}$ is the relative permittivity on the xz-plane and, therefore, $\epsilon_t^{(i)} = \epsilon_{xx}^{(i)} = \epsilon_{zz}^{(i)}$. The sides of the rectangular shield may be chosen as electric or magnetic walls so as to simulate a closed or an open structure.

The dispersive properties of structures, such as those shown in Fig. 1, are obtained by solving Maxwell's equations in terms of LSE and LSM modes in the Fourier domain [5]. In this case, the finite even–odd-mode Fourier representation of the electromagnetic field is adopted by erecting a symmetric magnetic or electric wall at the plane $x = 0$. For the geometries of Fig. 1, the finite Fourier transforms are defined in each layer as

$$\tilde{\mathscr{E}}_y^{\mathrm{TM}}(k_n) = \int_0^a E_y^{\mathrm{TM}}(x) \begin{matrix}\cos\\ \sin\end{matrix}(k_n x)\, dx \tag{2}$$

and

$$\tilde{\mathscr{H}}_y^{\mathrm{TE}}(k_n) = \int_0^a H_y^{\mathrm{TE}}(x) \begin{matrix}\sin\\ \cos\end{matrix}(k_n x)\, dx \tag{3}$$

where the upper case corresponds to a magnetic and the lower case to an electric wall at $x = 0$. The choice of k_n also enforces a magnetic and electric wall at $x = a$, that is, at the side wall. The combination of (2) and (3) and k_n leads to an open or closed structure, when k_n is chosen as $n\pi/a$ or $(2n-1)\pi/2a$, respectively. If the lower case of (2)

0018-9480/85/1200-1436$01.00 ©1985 IEEE

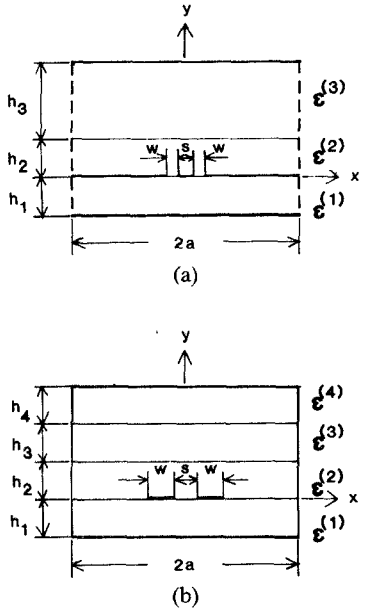

Fig. 1. Coplanar waveguide and coupled microstrip geometries on anisotropic layers. (a) Coplanar waveguide. (b) Coupled microstrip.

and (3) and $k_n = n\pi/a$ are chosen, then this corresponds to the odd-mode for the coupled microstrip lines or to a single microstrip line in the closed waveguide geometry. The other combination generates the case for an open side-wall geometry and it is useful for simulating an open structure for slot lines or other waveguiding systems.

LSE Modes

$$\tilde{\mathscr{E}}_x^{\mathrm{TE}} = \frac{\omega\mu_0\beta}{\beta^2 + k_n^2}\tilde{\mathscr{H}}_y^{\mathrm{TE}} \tag{4}$$

$$\tilde{\mathscr{E}}_z^{\mathrm{TE}} = \pm\frac{j\omega\mu_0 k_n}{\beta^2 + k_n^2}\tilde{\mathscr{H}}_y^{\mathrm{TE}} \tag{5}$$

$$\tilde{\mathscr{H}}_x^{\mathrm{TE}} = \pm\frac{k_n}{\beta^2 + k_n^2}\frac{\partial\tilde{\mathscr{H}}_y^{\mathrm{TE}}}{\partial y} \tag{6}$$

and

$$\tilde{\mathscr{H}}_z^{\mathrm{TE}} = \frac{-j\beta}{\beta^2 + k_n^2}\frac{\partial\tilde{\mathscr{H}}_y^{\mathrm{TE}}}{\partial y} \tag{7}$$

where $\tilde{\mathscr{H}}_y^{\mathrm{TE}}$ satisfies the wave equation

$$\frac{\partial^2\tilde{\mathscr{H}}_y^{\mathrm{TE}}}{\partial y^2} - \left[k_n^2 + \beta^2 - \epsilon_t k_0^2\right]\tilde{\mathscr{H}}_y^{\mathrm{TE}} = 0. \tag{8}$$

LSM Modes

$$\tilde{\mathscr{E}}_x^{\mathrm{TM}} = \pm\frac{k_n(\epsilon_{yy}/\epsilon_t)}{\beta^2 + k_n^n}\frac{\partial\tilde{\mathscr{E}}_y^{\mathrm{TM}}}{\partial y} \tag{9}$$

$$\tilde{\mathscr{E}}_z^{\mathrm{TM}} = -\frac{j\beta(\epsilon_{yy}/\epsilon_t)}{\beta^2 + k_n^2}\frac{\partial\tilde{\mathscr{E}}_y^{\mathrm{TM}}}{\partial y} \tag{10}$$

$$\tilde{\mathscr{H}}_x^{\mathrm{TM}} = -\frac{\epsilon_0\epsilon_{yy}\beta}{\beta^2 + k_n^2}\tilde{\mathscr{E}}_y^{\mathrm{TM}} \tag{11}$$

and

$$\tilde{\mathscr{H}}_z^{\mathrm{TM}} = \pm\frac{j\omega\epsilon_0\epsilon_{yy}k_n}{\beta^2 + k_n^2}\tilde{\mathscr{E}}_y^{\mathrm{TM}} \tag{12}$$

where $\tilde{\mathscr{E}}_y^{\mathrm{TM}}$ satisfies the wave equation

$$\frac{\partial^2\tilde{\mathscr{E}}_y^{\mathrm{TM}}}{\partial y^2} - \left(\frac{\epsilon_t}{\epsilon_{yy}}\right)\left[k_n^2 + \beta^2 - \epsilon_{yy}k_0^2\right]\tilde{\mathscr{E}}_y^{\mathrm{TM}} = 0. \tag{13}$$

The solution to the multiple boundary layer problem yields

$$\begin{bmatrix} j\tilde{\mathscr{J}}_x \\ -\tilde{\mathscr{J}}_z \end{bmatrix} = \begin{bmatrix} H_{11} & H_{12} \\ H_{21} & H_{22} \end{bmatrix}\begin{bmatrix} j\tilde{\mathscr{E}}_z \\ \tilde{\mathscr{E}}_x \end{bmatrix} \tag{14}$$

or inversely

$$\begin{bmatrix} j\tilde{\mathscr{E}}_z \\ \tilde{\mathscr{E}}_x \end{bmatrix} = \begin{bmatrix} G_{11} & G_{12} \\ G_{21} & G_{22} \end{bmatrix}\begin{bmatrix} j\tilde{\mathscr{J}}_x \\ -\tilde{\mathscr{J}}_z \end{bmatrix} \tag{15}$$

where $\tilde{\mathscr{J}}_x$ and $\tilde{\mathscr{J}}_z$ are finite Fourier transforms for the metallic strip current density components and $\tilde{\mathscr{E}}_z$ and $\tilde{\mathscr{E}}_x$ represent the finite Fourier transforms of the slot aperture electric-field components. The various terms involved in (16) and (17) are given by

$$H_{11} = H_{22} = \pm\left(\frac{\omega\epsilon_0}{k_0}\right)\frac{k_n\beta}{\gamma_n^2}\left[F_1(k_n,\beta) + F_2(k_n,\beta)\right] \tag{16}$$

$$H_{12} = \left(\frac{\omega\epsilon_0}{k_0}\right)\frac{1}{\gamma_n^2}\left[\beta^2 F_1(k_n,\beta) - k_n^2 F_2(k_n,\beta)\right] \tag{17}$$

$$H_{21} = \left(\frac{\omega\epsilon_0}{k_0}\right)\frac{1}{\gamma_n^2}\left[k_n^2 F_1(k_n,\beta) - \beta^2 F_2(k_n,\beta)\right] \tag{18}$$

$$G_{11} = H_{22}/\Delta \qquad G_{12} = -H_{12}/\Delta$$
$$G_{21} = -H_{21}/\Delta \quad \text{and} \quad G_{22} = H_{11}/\Delta \tag{19}$$

where

$$\Delta = H_{11}H_{22} - H_{12}H_{21}. \tag{20}$$

In addition

$$F_1(k_n,\beta) = \left[1/f_{t1} + \left(\alpha_t^{(2)^2} f_{t2} f_{t3} + 1\right)/(f_{t2} + f_{t3})\right] \tag{21}$$

$$F_2(k_n,\beta) = \left[1/g_{y1} + \left(g_{y2}g_{y3} + \alpha_y^{(2)^2}\right)/\left\{\alpha_y^{(2)^2}(g_{y2} + g_{y3})\right\}\right] \tag{22}$$

$$\gamma_n^2 = \beta^2 + k_n^2 \tag{23}$$

$$\alpha_y^{(i)} = \sqrt{\left\{(\gamma_n/k_0)^2 - \epsilon_y^{(i)}\right\}/\left(\epsilon_y^{(i)}\epsilon_t^{(i)}\right)} \tag{24}$$

$$\alpha_t^{(i)} = \sqrt{(\gamma_n/k_0)^2 - \epsilon_t^{(i)}} \tag{25}$$

$$f_{ti} = \tanh\left(k_0\alpha_t^{(i)}h_i\right)/\alpha_t^{(i)} \tag{26}$$

$$g_{yi} = \alpha_y^{(i)}\tanh\left(\epsilon_t^{(i)}k_0\alpha_y^{(i)}h_t\right). \tag{27}$$

The choice between (16) and (17) depends on whether the structure of Fig. 1(a) or (b) is considered, respectively. Since duality applies, the expansion functions for $E_x(x)$ and $J_z(x)$ may be chosen alike. Similarly, this is true for

$E_x(x)$ and $J_x(x)$. For the former case, the chosen field or current distribution satisfies the edge condition, i.e., the expansion functions are selected to obey the Maxwell functional dependence across the aperture or across the metallic strip, while for the latter case, the chosen expansion functions are like sinusoids forced to zero value at the slot or metallic strip edges. In the application of the Galerkin method, a variety of expansion functions, such as Legendre polynomials, Chebyshev polynomials, and pulse functions, have been employed in conjunction with the Maxwell dependence to satisfy the edge condition, and to represent $E_x(x)$ on a slot or $J_z(x)$ on a metallic strip. These choices lead to solutions which involve special functions such as Bessel functions. Solutions in terms of special functions typically increase the required CPU time and therefore decrease the efficiency of the algorithm. To enhance the algorithm efficiency, a simple polynomial expansion is made for $E_x(x)$ or $J_z(x)$ and sine basis functions are chosen for the $E_z(x)$ or $J_x(x)$ distributions. These polynomial expansions introduce further numerical simplifications since simple recurrence relations may be developed, thereby contributing to further minimization of CPU computation time.

The aperture field or metallic strip current representations are chosen as

$$\begin{Bmatrix} E_x(x) \\ -J_z(x) \end{Bmatrix} = \sum_{k=1}^{N} C_k f_k(x) \tag{28}$$

and

$$\begin{Bmatrix} jE_z(x) \\ jJ_x(x) \end{Bmatrix} = \sum_{k=1}^{M} D_k g_k(x) \tag{29}$$

where

$$f_k(x) = \left(\frac{x - s/2 - w/2}{w/2} \right)^{k-1}$$

and

$$g_k(x) = \sin\left(k\pi \frac{x - s/2}{w/2} \right). \tag{30}$$

Application of the Galerkin method yields a system of $(N+M)\times(N+M)$ eigenequations to be solved. The dispersion relation for ϵ_{eff} as a function of β/k_0 is obtained by solving the determinant

$$\begin{bmatrix} X_{i,k}^{1,1} & X_{i,k}^{1,2} \\ X_{i,k}^{2,1} & X_{i,k}^{2,2} \end{bmatrix} = 0 \tag{31}$$

where each element is given for the magnetic wall case at the center by

$$\begin{bmatrix} X_{i,k}^{1,1} \\ X_{i,k}^{1,2} \\ X_{i,k}^{2,1} \\ X_{i,k}^{2,2} \end{bmatrix} = \sum_{n=1}^{\infty} \begin{bmatrix} \tilde{f}_i^s H_{11} \tilde{g}_k^c \\ \tilde{g}_i^c H_{12} \tilde{g}_k^c \\ \tilde{f}_i^s H_{21} \tilde{f}_k^s \\ \tilde{g}_i^c H_{22} \tilde{f}_k^s \end{bmatrix} \tag{32}$$

for slots, while for microstrip structures

$$\begin{bmatrix} X_{i,k}^{1,1} \\ X_{i,k}^{1,2} \\ X_{i,k}^{2,1} \\ X_{i,k}^{2,2} \end{bmatrix} = \sum_{n=1}^{\infty} \begin{bmatrix} \tilde{f}_i^c G_{11} \tilde{g}_k^s \\ \tilde{g}_i^s G_{12} \tilde{g}_k^s \\ \tilde{f}_1^c G_{21} \tilde{f}_k^c \\ \tilde{g}_i^s G_{22} \tilde{f}_k^c \end{bmatrix}. \tag{33}$$

The " $\sim$ " symbol in (33) indicates the Fourier transformed basis functions given by (28) and (29). A recurrence relation can be easily derived for these Fourier transforms.

Thus, the recurrence relations of the $f_k^{(x)}$ basis functions are derived as

$$\begin{aligned} \tilde{f}_k^s(k_n) = {} & \frac{1}{k_n}\Big[(-1)^{k-1}\cos(k_n s/2) \\ & - \cos\{k_n(w+s/2)\}\Big] \\ & + \frac{(k-1)}{k_n^2 w/2}\Big[\sin\{k_n(w+s/2)\} \\ & - (-1)^{k-2}\sin(k_n s/2)\Big] \\ & - \frac{(k-1)(k-2)}{(k_n w/2)^2}\tilde{f}_{k-2}^s(k_n) \end{aligned} \tag{34}$$

for the sine Fourier transform and

$$\begin{aligned} f_k^c(k_n) = {} & \frac{1}{k_n}\Big[\sin\{k_n(w+s/2)\} \\ & - (-1)^{k-1}\sin(k_n s/2)\Big] \\ & - \frac{(k-1)}{k_n^2 w/2}\Big[(-1)^{k-2}\cos(k_n s/2) \\ & - \cos\{k_n(w+s/2)\}\Big] \\ & - \frac{(k-1)(k-2)}{(k_n w/2)^2}\tilde{f}_{k-2}^c(k_n) \end{aligned} \tag{35}$$

for the corresponding cosine Fourier transform.

It is observed that the choice of the $\{f_k(x)\}$ set yields recurrence relations in the Fourier domain which consist of simple sine and cosine functions, thereby contributing to the development of an efficient numerical algorithm. It is also interesting to note that a Maxwell distribution may be approximated readily with 6 or 7 basis function terms.

III. Characteristic Impedance

The characteristic impedance for microstrip is computed in this section by considering the definition $Z_0 = V(k_0)/I(k_0)$. For this calculation, the voltage and longitudinal current are given by

$$V(k_0) = -\int_{-h_1}^{0} E_y dy \tag{36}$$

and

$$I(k_0) = \sum_{n=1}^{N} \frac{2C_n}{n} \tag{37}$$

TABLE I

$2b/h_1$	h_2/h_1	s/h_1	w/h_1	Phase velocity	Ref [2]	Dynamic solution
6.2	0.8	1.6	0.58	v_{ph}^e	0.9629	0.9632
				v_{ph}^o	0.9646	0.9647
12.0	2.0	1.6	0.55	v_{ph}^e	0.9323	0.9324
				v_{ph}^o	0.9333	0.9333

respectively. This definition of Z_0 has been compared with the results reported for a single microstrip line on sapphire, and the agreement is excellent [8]. Also, a comparison with the computation for Z_0^e, Z_0^o for coupled microstrip lines on isotropic substrates [9], as computed by using the definition $Z_0 = 2P/I^2$, yields a 0.5-percent difference for higher frequencies and a 1.4-percent difference for lower frequencies for both the even- and odd-mode cases (see Fig. 6). This algorithm has also been tested against quasi-static calculations [1] with an agreement better than 0.1 percent.

IV. Numerical Results and Discussion

The results obtained with the algorithm developed in this article are within 0.5-percent convergence accuracy. Table I makes a comparison of the algorithm developed herein with the quasi-static results for coupled microstrip with cover on a sapphire substrate with an alumina overlay [2]. For this case, reference to Fig. 1(b) indicates that $\epsilon_{xx}^{(1)} = 9.4$, $\epsilon_{yy}^{(1)} = 11.6$, $\epsilon_{xx}^{(2)} = \epsilon_{yy}^{(2)} = 9.9$, while $\epsilon_{xx}^{(3)} = \epsilon_{xx}^{(4)} = \epsilon_{yy}^{(3)} = \epsilon_{yy}^{(4)} = 1$. To simulate a structure which is open on the sides, the dimension $2a$ has been chosen as 20. The results shown in Table I indicate agreement to within 0.05 percent between the two methods for both even- and odd-mode phase velocities. For these computations, the choice $N = 2$, $M = 10$, and $n_{sum} = 1000$ yields 0.05-percent convergence accuracy.

Fig. 2(a) demonstrates the dispersive behavior of λ_g/λ_0 for coupled slotlines on a saphire substrate. Comparison of this result with the dispersive behavior of coupled slots as obtained by the equivalent network method [6] indicates no visible discrepancy between the two methods. For this particular case $N = 6$, $M = 6$, $N_{sum} = 300$, and in order to simulate an open structure $2a = 20$ while $2b = 21$. In addition, it is observed that the dominant mode (odd mode) is obtained with electric side walls at $x = \pm a$, while the even mode results if the side walls at $x = \pm a$ are perfect magnetic conductors. Fig. 2(b) compares the ϵ_{eff} for even and odd modes for an Epsilam-10 substrate when anisotropy is accounted for or when it is neglected. It is clearly observed that with increasing frequency, the error when anisotropy is neglected increases. For the dominant mode, it is observed that it is 11.6 percent at low frequencies ($k_0 h_2 \doteq 0$) and it increases to 13.3 percent when $k_0 h_2 = 0.6$. This example demonstrates the significance of including substrate anisotropy in the development of highly accurate design algorithms for microwave and millimeter-wave circuits. Fig. 3 illustrates the dispersive behavior of

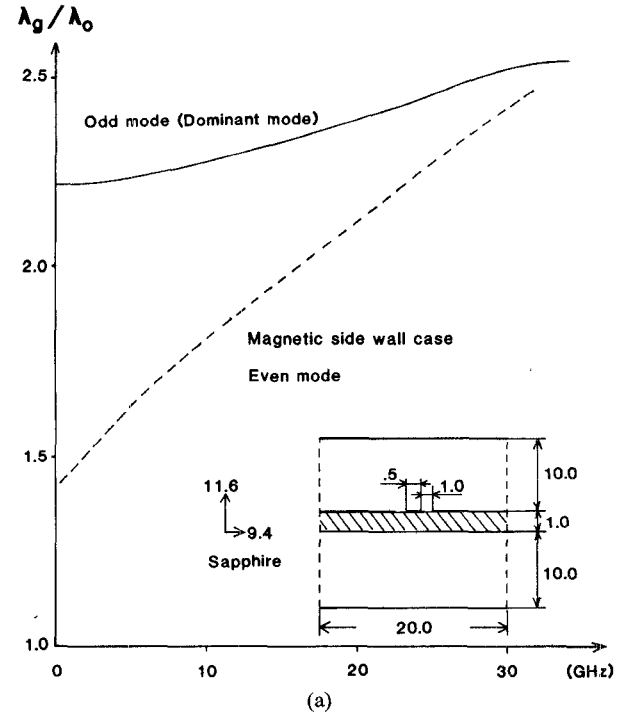

(a)

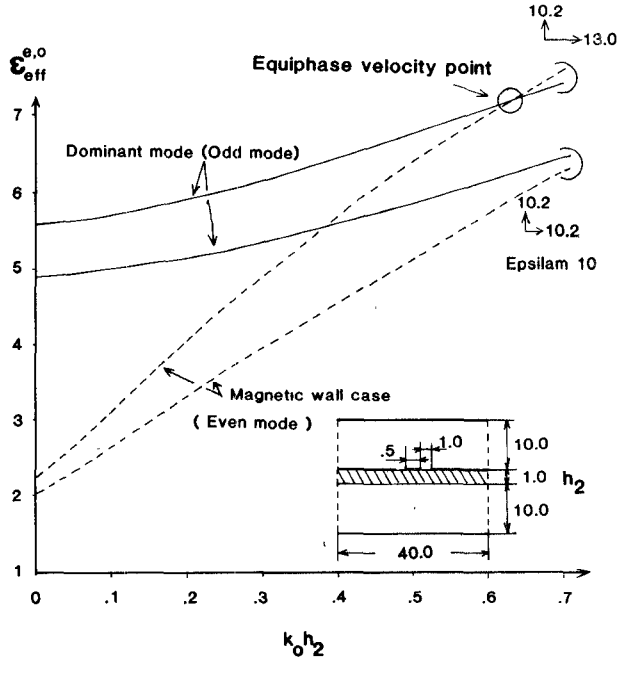

(b)

Fig. 2. (a) Dispersion characteristics of coupled slotlines on sapphire substrate. (b) Dispersion characteristics of coupled slotlines.

ϵ_{eff} for a slotline on sapphire. Of interest in this particular case are the waveguide modes shown in dashed lines. The first waveguide mode is generated by the substrate-filled portion of the waveguide, while the second, by the entire structure. The cutoff frequencies for these modes may be predicted by considering the ϵ_{eff}-filled waveguide mode and the transverse resonance method. The results are obtained as $k_{01} = 0.97$ with $\epsilon_{eff} = \sqrt{\epsilon_t \epsilon_y} = 10.44$. Also, the

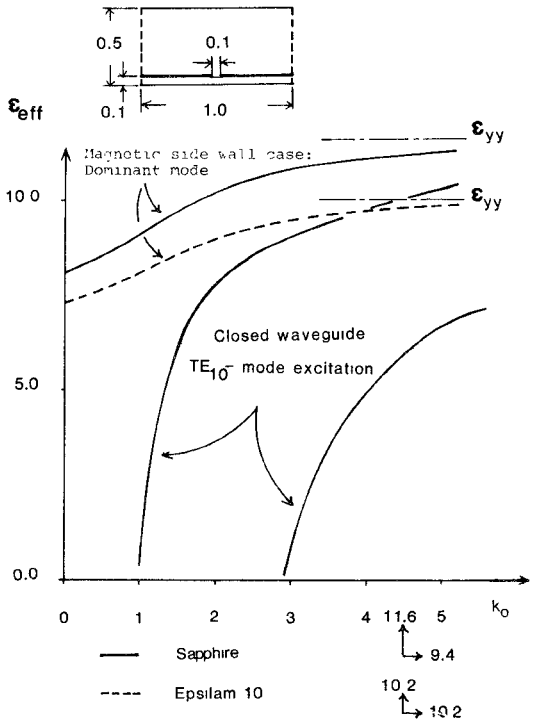

Fig. 3. Dispersion characteristics of single slotline for open and closed geometry.

TABLE II
C_k VALUES

Even mode	Odd mode
.2477	.0869
.0883	−.0494
.0518	.1895
−.2894	.1728
−.3373	−.7139
.5113	−.2935
1.0	1.0

transverse resonance method approximates k_{c2} here as

$$k_{c2} \sim \frac{\pi}{b}\left(\frac{\epsilon_{\text{eff}}(a-d)+d}{\epsilon_{\text{eff}}a}\right) \sim 2.84$$

which agrees with the computed result. In the above expression, a is the width, b is the height, and d is the substrate thickness.

The comparison to Epsilam 10 has also been shown for the magnetic wall case; an open structure is simulated. The dominant mode for this case exhibits a y-directed field component dominated by the ϵ_{yy} factor. The computed result shows the asymptotic behavior of the effective dielectric constant to the ϵ_{yy} component of the permittivity tensor.

Fig. 6 demonstrates the comparison to El-Sherbiny's results [8]. The effective dielectric constant and characteristic impedance show excellent agreement. The current distribution for low frequency is also shown where seven basis functions have been chosen here. The current density approximates the Maxwell current distribution with excellent agreement.

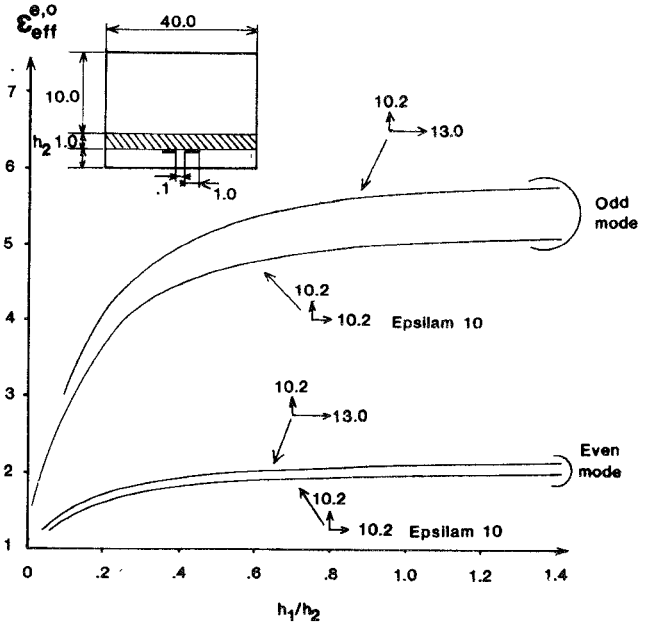

Fig. 4. Quasi-static characteristics of inverted microstrip lines.

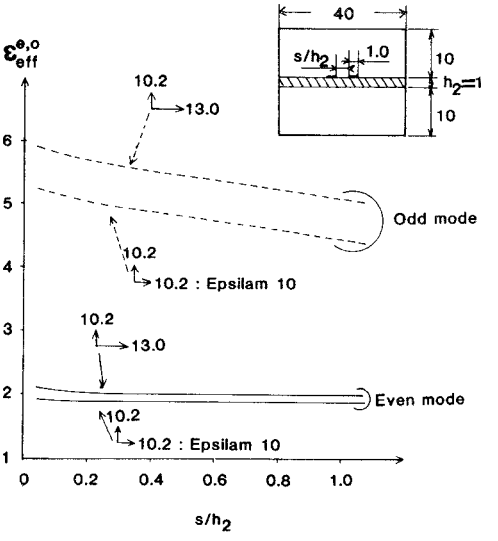

Fig. 5. Quasi-static properties of suspended microstrip lines.

The polynomial coefficients C_k are found as shown in Table II. Table I demonstrates that this choice of a simple set of basis functions yields excellent results for the current distribution while at the same time it provides for a very efficient numerical algorithm.

Finally, in order to emphasize the versatility of this technique, the low-frequency behavior of ϵ_{eff} is demonstrated in Figs. 4 and 5 for inverted coupled microstrip and for suspended coupled microstrip lines on isotropic and anisotropic Epsilam-10 substrates.

V. CONCLUSION

This paper presents a generalized approach to analyze the dispersive properties of integrated circuit structures on multiple layers of anisotropic materials. The algorithm developed by this method includes as limiting cases geome-

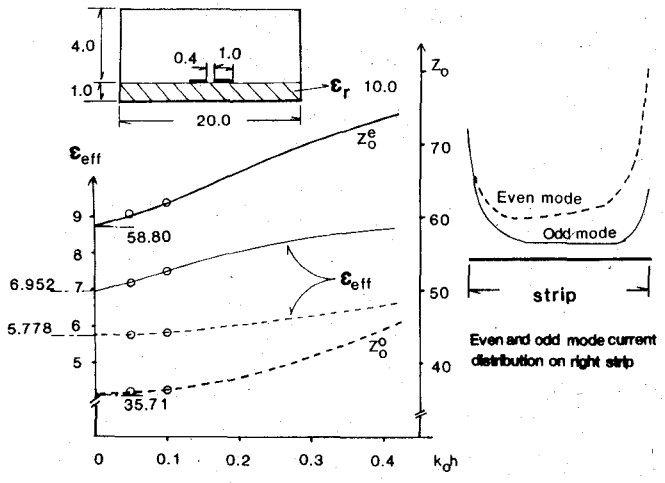

Fig. 6. Frequency-dependent characteristics of single microstrip line. ——— Even mode. ---- Odd mode. ∘ Reference: Fig. 16 and Fig. 17 [9].

tries of integrated waveguiding structures with or without cover, as well as the case of a rectangular shield. The results presented in this paper are within 0.5-percent convergence accuracy. Finally, it has been demonstrated that neglecting substrate anisotropy leads to serious errors in the effort to derive an accurate integrated circuit model.

References

[1] N. G. Alexopoulos, "Integrated circuit structures on anisotropic substrates," *IEEE Trans. Microwave Theory Tech.*, vol. MTT-33, pp. 847–881, Oct 1985.

[2] N. G. Alexopoulos and C. M. Krowne, "Characteristics of single and coupled microstrips on anisotropic substrates," *IEEE Trans. Microwave Theory Tech.*, vol. MTT-26, pp. 387–393, June 1978.

[3] N. G. Alexopoulos and S. Maas, "Characteristics of microstrip directional couplers on anisotropic substrates," *IEEE Trans. Microwave Theory Tech.*, vol. MTT-30, pp. 1267–1270, Aug. 1982.

[4] J. E. Mariki, "Analysis of microstrip lines on inhomogeneous anisotropic substrates by the TLM technique," Ph.D. dissertation, Univ. of California, Los Angeles, 1978.

[5] K. Shibata and K. Hatori, "Dispersion characteristics of coupled microstrip with overlay on anisotropic dielectric substrate," *Electron. Lett.*, Jan. 1984.

[6] T. Kitazawa and Y. Hayashi, "Coupled slots on an anisotropic sapphire substrate," *IEEE Trans. Microwave Theory Tech.*, vol. MTT-29, pp. 1035–1040, Oct. 1981.

[7] T. Kitazawa and Y. Hayashi, "Quasi-static characteristics of coplanar waveguide on a sapphire substrate with its optical axis inclined," *IEEE Trans. Microwave Theory Tech.*, vol. MTT-30, pp. 920–922, June 1982.

[8] A. Abdel-Moniem El-Sherbiny, "Hybrid mode analysis of microstrip lines on anisotropic substrates," *IEEE Trans. Microwave Theory Tech.*, vol. MTT-29, pp. 1261–1265, Dec. 1981.

[9] K. Krage and I. Haddad, "Frequency-dependent characteristics of microstrip transmission lines," *IEEE Trans. Microwave Theory Tech.*, vol. MTT-20, pp. 678–688, Oct. 1972.

[10] T. Kitazawa and Y. Hayashi, "Propagation characteristics of striplines with multilayered anisotropic media," *IEEE Trans. Microwave Theory Tech.*, vol. MTT-31, pp. 429–433, June 1983.

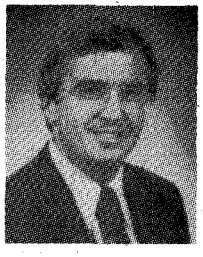

Nicólaos G. Alexópoulos (S'68–M'69–SM'82) was born in Athens, Greece, in 1942. He graduated from the 8th Gymnasium of Athens, Greece, and subsequently obtained the B.S.E.E., M.S.E.E., and Ph.D. degrees from the University of Michigan, Ann Arbor, MI, in 1964, 1967, and 1968, respectively.

He is currently a Professor in the Department of Electrical Engineering, University of California, Los Angeles, and a Consultant with Northrop Corporation's Advanced Systems Division. His current research interests are in electromagnetic theory as it applies in the modeling of integrated-circuit components and printed circuit antennas for microwave and millimeter-wave applications, substrate materials and their effect on integrated-circuit structures and printed antennas, integrated-circuit antenna arrays, and antenna concealment studies. He is the Associate Editor of the IEEE TRANSACTIONS ON ANTENNAS AND PROPAGATION, *Electromagnetics Journal*, and *Alta Frequenza*.

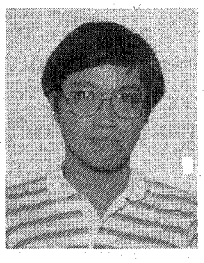

Akifumi Nakatani (S'81) was born in Tokyo, Japan, on February 10, 1956. He received the B.S.E.E. degree from Iwate University, Iwate, Japan, and the M.S.E.E. degree from Oregon State University in 1979 and 1981, respectively. He is currently studying at the University of California, Los Angeles, for the Ph.D. degree. His research interests include computer-aided analysis and design of microwave and millimeter-wave components and printed-circuit antennas.